

# Proceedings of Meetings on Acoustics

## Monitoring bubble production in a seagrass meadow using a source of opportunity --Manuscript Draft--

<b>Manuscript Number:</b>	
<b>Full Title:</b>	Monitoring bubble production in a seagrass meadow using a source of opportunity
<b>Article Type:</b>	ASA Meeting Paper
<b>Corresponding Author:</b>	Paulo Felisberto LARSyS, University of Algarve Faro, N/A PORTUGAL
<b>Order of Authors:</b>	Paulo Felisberto Orlando Camargo Rodríguez João Parente Silva Sérgio Jesus Hugo Quental Ferreira Pedro Pousão Ferreira Maria Emília Cunha Carmen B. de los Santos Irene Olivé Rui Santos
<b>Abstract:</b>	<p>Under high irradiance, the photosynthetic activity of dense seagrass meadows saturates the water forming oxygen bubbles. The diel cycle of bubble production peaks at mid-day, following light intensity pattern. It is well known that bubbles strongly affect the acoustic propagation, increasing signal attenuation and decreasing the effective water sound speed, noticeable at low frequencies. Thus, the diurnal variability of bubbles may show an interference pattern in the spectrograms of low frequency acoustic signals. In an experiment conducted in July 2016 at the Aquaculture Research Station of the Portuguese Institute for the Sea and Atmosphere in Olhão, Portugal, the spectrograms of low frequency (&lt;20kHz) broadband noise produced by water pumps in a pond of 0.48ha covered by the seagrass <i>Cymodocea nodosa</i> showed interference patterns that can be ascribed to the variability of the sound speed in the water. Preliminary analysis suggests that the daily cycle of bubble concentration can be inferred from these interference patterns.</p>
<b>Section/Category:</b>	Acoustical Oceanography

# **Monitoring bubble production in a seagrass meadow using a source of opportunity**

P. Felisberto, O.C. Rodríguez, J.P. Silva, S. Jesus,<sup>1</sup>

H. Quental-Ferreira, P. Pousão-Ferreira, M. Cunha,<sup>2</sup>

C.B. de los Santos, I. Olivé, R. Santos.<sup>3</sup>

1 - LARSyS, University of Algarve, Faro, PORTUGAL

2 - IPMA - Instituto Português do Mar e da Atmosfera,  
EPPO, Olhão, PORTUGAL

3 - Marine Plant Ecology research group, Center of  
Marine Sciences of University of Algarve, Faro, PORTUGAL|

---

## INTRODUCTION

Seagrass are marine plants living in coastal areas from foreshore to depths of few tens of meters. Seagrass beds contain a large biodiversity, prevent erosion of the seabed, store carbon dioxide and produce large amounts of oxygen (O<sub>2</sub>) by photosynthesis. The photosynthetic activity of seagrass gives rise to a build-up of oxygen pools inside the tissues and in leaf lacunae.<sup>1</sup> The oxygen produced by photosynthesis is released to the water column by diffusion. However, under supersaturation conditions bubbles are formed at the surface of leaves; bubble streams from damaged leaves have also been noticed.<sup>2</sup> Therefore, bubbles can be used as a proxy of the status of the seagrass bed. It is well known that bubbles have a significant impact on acoustic propagation giving rise to an excess signal attenuation at frequencies close to bubbles resonance.<sup>3</sup> The resonance frequency of a bubble is inverse to its radius. At 1 m depth, the resonance frequency of bubbles of 0.6 mm and 60  $\mu$ m radius are approximately 6 kHz and 60 kHz, respectively. The acoustic propagation in bubbly media is dispersive, but for low frequencies (compared with bubbles resonance frequency) and small concentration of bubbles, one can rely on Wood's equation,<sup>3</sup> which relates the bubbles void fraction (the ratio of bubbles volume to the liquid volume) to the effective sound speed of the bubbly media. Generally speaking, an increase of the bubbles void fraction gives rise to a decrease of the effective sound speed of the media. Methods based on the measurement of the travel time anomalies have been used to determine bubbles void fraction, for example from bubbles originated beneath the surface by wind.<sup>4</sup> However, in this paper we use a different approach based on the interference patterns (striations) visible in the spectrograms due to the variability of environmental parameters, such a range, water depth, or (in the present case) sound speed. The applicability of these methods relying on broadband noise sources has been proven (see Kinda and Bonnel<sup>5</sup> and references within).

In this work we use broadband noise (<26 kHz), generated by a water pump installed in a very shallow pond (water depth <2.5 m), to track the bubbles production of a seagrass bed that covers the bottom. The experiment was conducted during 2 diel cycles in summer conditions, when supersaturation occurred during daylight. The interference patterns observed in the photosynthetic active period might be ascribed to the variability of the effective sound speed of the water, due to gas bubbles. Particularly, interferences in the band 2–7.5 kHz have been used to obtain a rough estimate of the bubbles void fraction. However, the acoustic propagation in the pond was also largely affected by the variability of water depth due to the tide. In the lower frequency band (0.7–2 kHz), during the night, an interference pattern associated with the water depth variability was clearly seen. This paper starts with a description of the experimental setup and data acquisition. Then, we present the noise data, discuss their variability in the different frequency bands and the estimation of bubbles void fraction. Finally, we draw some conclusions.

## EXPERIMENTAL DATA COLLECTION

The data under consideration were collected from July 25th to 27th 2016 in a pond of the Aquaculture research station (EPPO) in the Ria Formosa lagoon area, Olhão, south of Portugal (see Fig. 1). The ponds and the channel are covered by seagrasses *Cymodocea nodosa*; the pond (a) is directly connected to the Ria Formosa through a tide gate. The acoustic measurements took place in pond (c) from which the water is pumped to various tanks in the research station. The ponds are connected by channel (b). The mean water depth at pond (c) is 1.7 m, ranging from 1.4 to 2.1 m.

The main contributions to acoustic noise in the pond is generated by the water pumps installed 30 cm from the bottom at the location labeled (c), indicated by the red arrow in Fig. 1(right). An aeration pump is installed close to the water pumps. The aeration pump was switched off in the first day, and switched on in the second.

*Cymodocea nodosa* covers the whole pond bottom with few, uncovered patches. The plants have an averaged leaf length of  $32.4 \pm 0.5$  cm. The bottom composition is unknown, but visual inspection revealed

---



**Figure 1:** EPPO areas with *Cymodocea nodosa*. Ponds (a) and (c) are interconnected by channel (b) and connected to Ria Formosa lagoon through a tide gate in pond (a) (left). The measurements were performed in pond (c) at the location indicated by the white arrow (right). The water pumps that feed the adjacent aquaculture tanks and station are installed in the corner indicated by label (C). The red arrow indicates the location of the water pumps. The foam is an indication that aeration pumps are working.

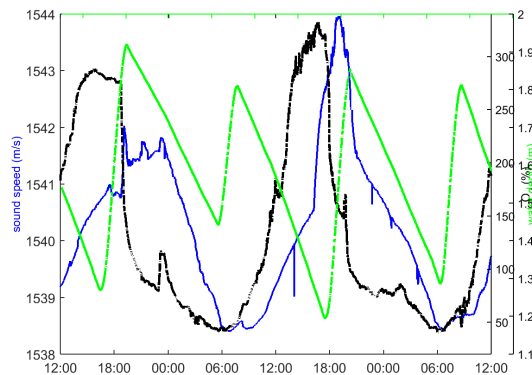


**Figure 2:** CTD data: sound speed (blue), dissolved oxygen (black) and water depth at the pressure sensor (green).

a thin sandy layer and anoxic sediments.

Acoustic data were acquired every 10 m by the MarSensing SR-1 hydrophone at a sampling frequency of 44.1 kHz. Complementary environmental data were acquired by a RBRconcerto CTD, that includes a Rinko optode to measure dissolved oxygen. The CTD data was acquired at a sampling frequency of 1 Hz. Both, hydrophone and CTD were moored at 60 cm from the bottom at the location indicated by the white arrow in Fig. 1(right). The distance between the water pumps (red arrow) and the hydrophone (white arrow) was approximately 35 m.

The most relevant environmental data for the analysis of the variability of the acoustic noise in the pond (sound speed, depth and dissolved oxygen) are presented in Fig. 2. The average sound speed was approximately 1540 m/s, showing a diurnal variability pattern with a minimum at 06:00 and a maximum at 18:00. The dissolved O<sub>2</sub> followed also a diurnal pattern with a minimum at 06:00. Afterwards, it rapidly increased until 13:30. Then, until 18:30 the variation is relatively small. After 18:30, dissolved oxygen rapidly decreased. The saturation level reached very high values: approximately 290% in the 1st diurnal cycle and more than 300% in the 2nd diurnal cycle. However, undersaturation occurred from 20:30 until

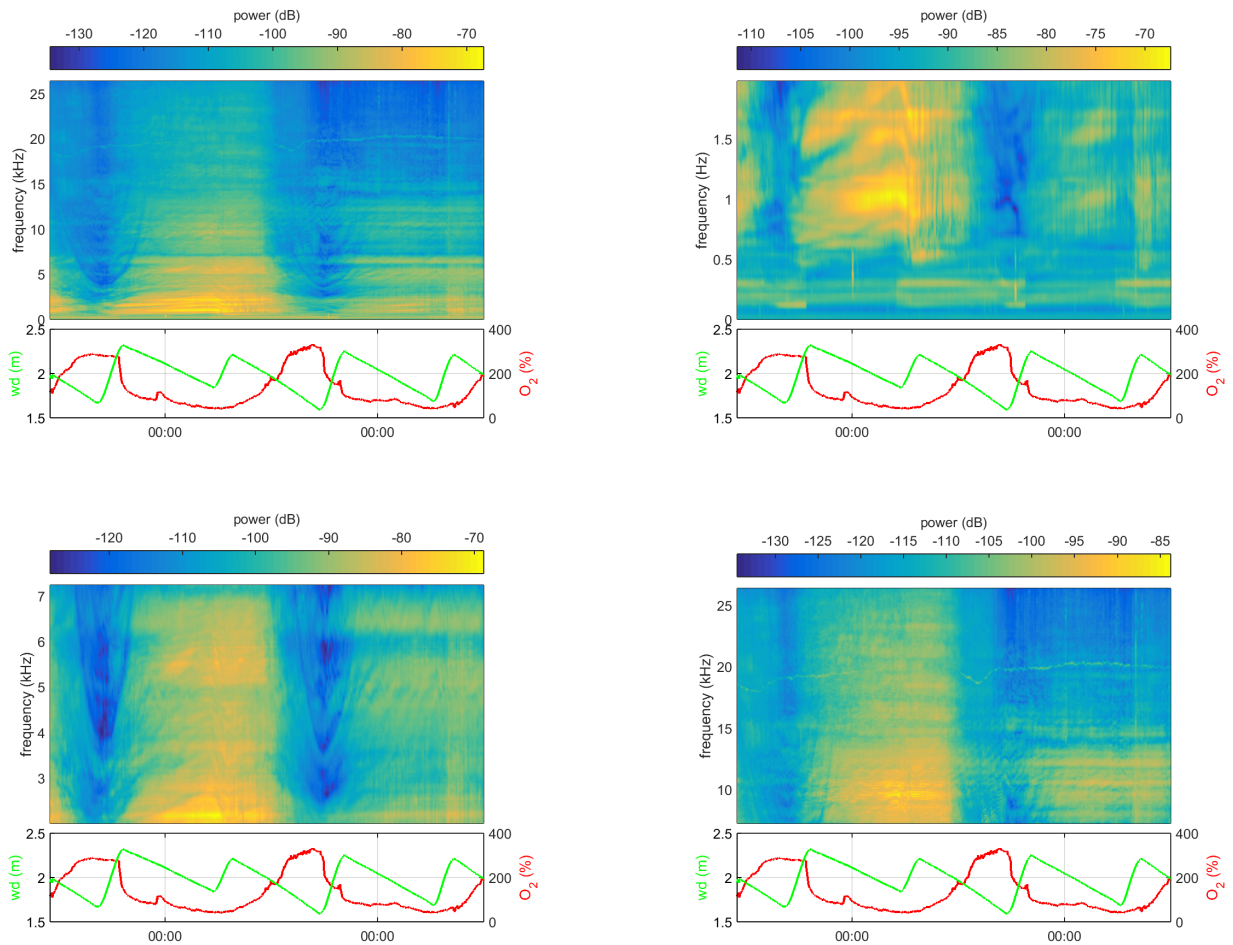


**Figure 3: Power spectral density of the ambient noise estimated every 10 min during 2 diurnal periods: full 0–25 kHz band (upper-left), and zoom of 0–2 kHz (upper-right), 2–7.25 kHz (bottom-left) and 7.25–25 kHz (bottom-right) bands. The red and green curves represent the O<sub>2</sub> saturation and water depth, respectively.**

10:00 next day, with a minimum value below 50% of the saturation level. The CTD depth varied with water flow due to tide. Due to the particular characteristics of the system of ponds and tide gate, the water depth increases and decreases almost linearly with a higher slope (faster) during the inflow. The instantaneous water depth at hydrophone mooring used in the next section was estimated by adding 60 cm to the CTD depth.

## NOISE PROCESSING AND ANALYSIS

The power spectral density of noise was computed using the Welch method from 30 s snapshots every 10 minutes using a 2048 points FFT with 512 samples overlapping. Figure 3 shows the power spectral density of the ambient noise along the 2 diurnal periods in the 0–25 kHz band and details of 0–2 kHz (upper-right), 2–7.25 kHz (bottom-left) and 7.25–25 kHz (bottom-right) bands, whereas the total power in each band is presented in Fig. 4. In both figures the O<sub>2</sub> saturation level and water depth are plotted as black and green

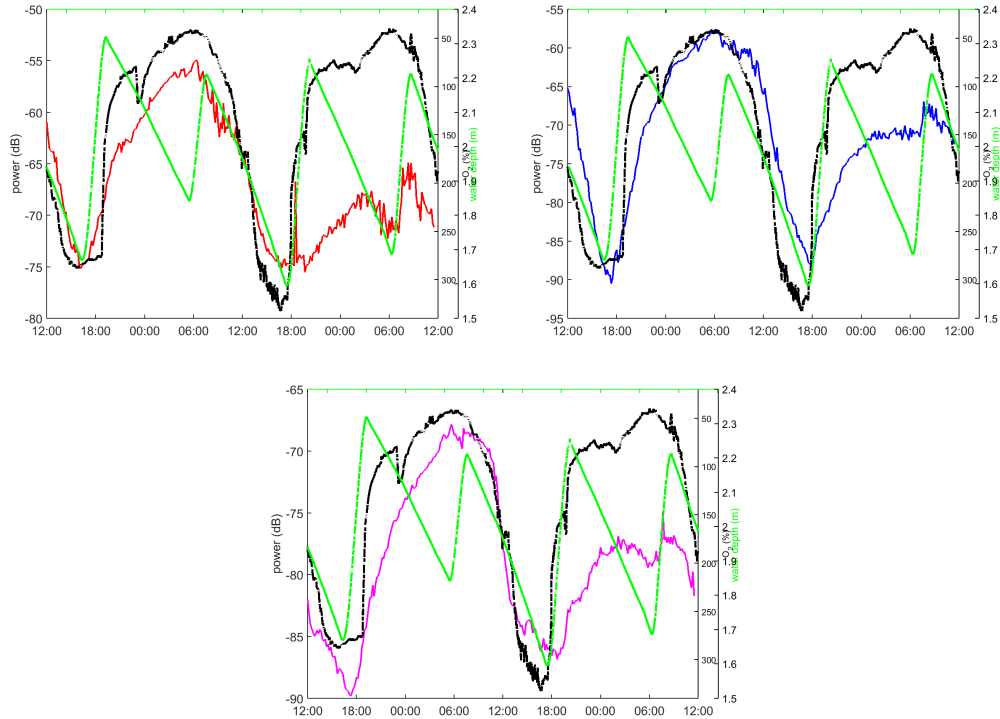


**Figure 4: Comparison between the variability of the noise power in the bands 0–2 kHz (red), 2–7.25 kHz (blue) and 7.25–25 kHz (magenta), and the variability of O<sub>2</sub> saturation level (black). The green line represents the water depth (estimated from CTD).**

lines, respectively. It can be seen that the attenuation of the ambient noise is high (daylight) when the O<sub>2</sub> saturation level is also high. Although, the periods of low O<sub>2</sub> saturation levels have similar extent and values, the noise power is significantly lower ( $\sim 15$  dB) during the second period. During this period the aeration pumps moored at a location close to the water pumps were working; thus, the bubbles produced by the aeration pumps most likely attenuated the acoustic noise generated by the water pumps.

Moreover, one can notice other distinguishing features, that are believed to be linked to the variability of the effective sound speed of water due to bubbles, and to the variability of water depth due to the tide. In both periods when the O<sub>2</sub> saturation achieves its maximum and then decreases one can notice striation patterns with a parabolic shape, particularly in the band 2–7.25 kHz. These striations may be linked to the change of effective sound speed of the media due to bubbles. In the period of highest level of ambient noise power (July 25, 18h to July 26, 6h), one can notice striation patterns in the band 0.4–2 kHz, with a shape that seems to be related to water depth variability, although with an inverted trend. During the next night period the ambient noise level is about 15 dB lower, the broadband component is highly attenuated and this striation pattern is not visible. These patterns are discussed next.

## STRIATION PATTERNS

Striations represent inter modal interference due to the variability of waveguide parameters. These striations are trends across frequencies, where the acoustic intensity (or power) is constant. Striations appear in the spectrograms of broadband signals, when the horizontal axis is associated with the variability of a particular waveguide parameter. Perhaps the best well known striation patterns are those associated with the variability of source-receiver range. Striation patterns associated with the variability of the water column

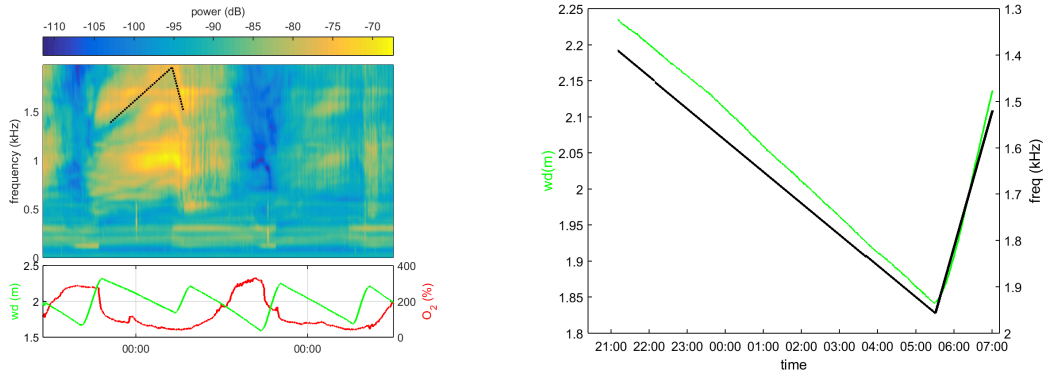


**Figure 5: Striation pattern due to water depth variability: spectrogram with superimposed striation curve (left), and comparison (right), where the black curve represents the striation and the green curve represents water depth.**

height have been reported in reference.<sup>5</sup> From the striations there have been derived simple relations between the frequency and the corresponding variable parameter. Kinda and Bonnel<sup>5</sup> have shown that for an isovelocity range-independent shallow water waveguide with depth  $D$  the striation is given by the relation

$$\frac{d\omega}{\omega} = -2 \frac{dD}{D} \quad (1)$$

where  $\omega$  is the frequency. Relying on shipping noise data both authors confirmed that there is indeed a high (anti) correlation between the striation pattern and the tide. Using a similar reasoning, the frequency-sound speed relation can be found to be

$$\frac{d\omega}{\omega} = \frac{dc}{c} \quad (2)$$

where  $c$  is the sound speed in the waveguide. As indicated by the expression one should expect that sound speed should decrease if the striation curve tends towards low frequencies, and vice-versa.

Striation patterns associated with water depth and sound speed can be seen in the dataset analyzed herein. Figure 5 illustrates the striation pattern due to water depth variability, which can be seen during the first night when the ambient noise is high and broadband. The striation curve selected manually from the spectrogram in Fig. 5(left) is compared in Fig. 5(right) with the water depth measured by the CTD in the same period, showing a good agreement. Similar striation patterns are also present in this period in frequencies above 500 Hz, and in the next night period, although their shapes are less clear due to high amplitude tonal contamination, and low amplitude of broadband components leading to gaps in the frequency spectrum.

Figure 6 illustrates striation curves that can be noticed when the O<sub>2</sub> saturation level is high, thus in conditions when bubbles should be released to the water column. The striation curves selected manually from the spectrogram in Fig. 6(left) are presented in Fig. 6(right), both centered at the corresponding minimum. The shape of these striation curves suggest a link between the variability of the effective sound speed of the waveguide and bubble production, as they seem correlated with O<sub>2</sub> saturation levels in oversaturation conditions.

The influence of the water depth variability on these striation patterns seems to be small because of the low effective sound speed of the medium, thus the striations can be a robust indicator of sound speed variability and a base for the estimation of bubbles.

A rough estimate of the gas fraction can be obtained from the time-frequency striation curves shown in Fig. 6 and the Woods equation as follows: Using a first order discretization of Eq.2, we can obtain the sound

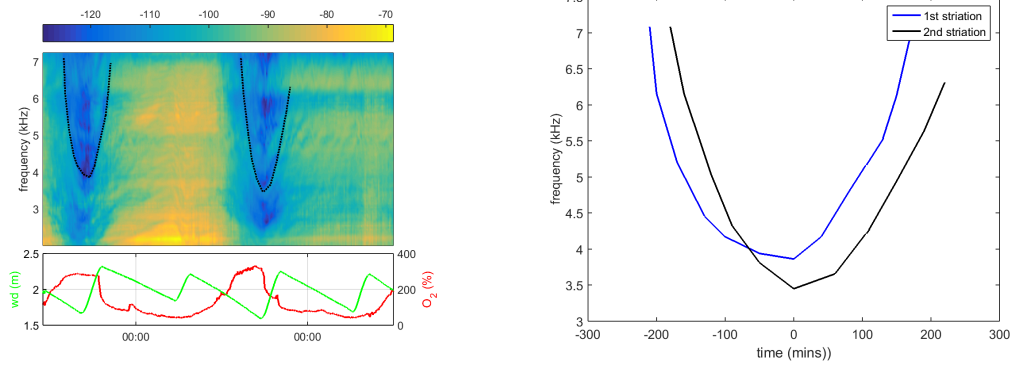


**Figure 6: Striation patterns due to sound speed variability: spectrogram with superimposed striation curves (left), comparison between the striation curves in the two periods.**

speed  $c_i$

$$c_i = c_{i-1} \frac{\omega_i}{\omega_{i-1}}, \quad i = 0, 1, \dots \quad (3)$$

where  $i$  is the time index of time-frequency striation curve, and  $\omega_i$ , is the corresponding frequency. We assume  $c_0$  as the bubble free water sound speed, 1540 m/s in the present case. Because of the linear relation, the time dependence of the effective sound speed has a shape similar to the time-frequency striation curve, with a minimum at the same time index. In the present case the minimum values of sound speed are 840 m/s and 750 m/s for the 1st and 2nd days, respectively.

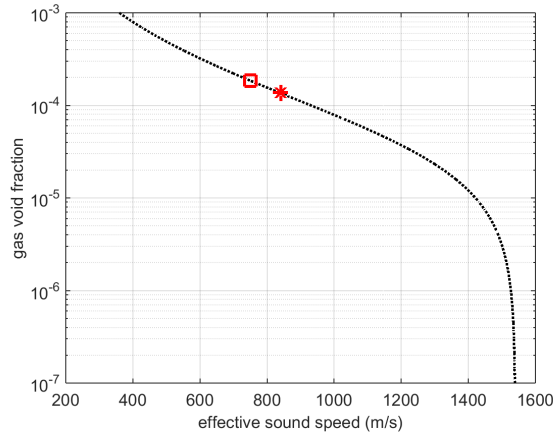


**Figure 7: Air bubbles void fraction as function of effective sound speed. The asterisk and square correspond to the minimum of the effective sound speed in the 1st and 2nd days, respectively.**

From Fig. 7, which relates the effective sound speed to the void fraction of the gas bubbles, we can estimate the gas void fraction to be approximately  $10^{-4}$  at peak values. These estimates are in close agreement with those presented in<sup>6</sup> using short range (1 m) transmissions of pulsed signals.

---

## CONCLUSION

This work showed that the photosynthetic activity of a *Cymodocea nodosa* meadow under oxygen supersaturation conditions significantly affects acoustic propagation, which can be ascribed to oxygen bubbles formation. Herein, in addition to oxygen bubbles formation, the water depth changes due to the tide have also a significant effect on acoustic propagation on a very shallow water pond. Noise generated by a water pump in the band 0–20 kHz was analyzed. In general, an excess attenuation was observed along the signal spectrum during the photosynthetic active period. However, a more detailed analysis shows particular effects at the different frequency bands. The interference patterns (striations) noticed in the band 2.5–7.5 kHz during the photosynthetic active period might be related to the change in effective sound speed of the water due gas bubbles concentration (void fraction). Using a simplified method to estimate the effective sound speed from the striations and assuming that the Wood's equation applies, an estimate of the gas void fraction of order of  $10^{-4}$  was obtained at peak production. It should be remarked that the effect of water depth changes on acoustic propagation is clearly seen as striation in the 0.4–2 kHz band during the night. This result corroborates earlier findings<sup>7</sup> of bubbles formation during photosynthesis in a *Posidonia oceanica* meadow.

## ACKNOWLEDGMENTS

This work was funded by National Funds through the Foundation for Science and Technology (FCT), under project PTDC/EEIPRO/2598/2014 (SEAOX). Acknowledgment is also due to MarSensing for lending the SR-1 hydrophone.

## REFERENCES

- <sup>1</sup> J. Borum, K. Sand-Jensen, T. Binzer, O. Pedersen, and T. M. Greve, *Oxygen Movement in Seagrasses*. Springer, 2006, pp. 255–270.
  - <sup>2</sup> C. J. Wilson, P. S. Wilson and K. H. Dunton, “An acoustic investigation of seagrass photosynthesis,” *Marine Biology*, vol. 159, no. 10, pp. 2311–2322, 2012.
  - <sup>3</sup> H. Medwin and C. S. Clay, “Chapter 8 - bubbles,” in *Fundamentals of Acoustical Oceanography*, H. Medwin and C. S. Clay, Eds. San Diego: Academic Press, 1998, pp. 287 – 347.
  - <sup>4</sup> E. Lamarre and W. K. Melville, “Instrumentation for the measurement of sound speed near the ocean surface,” *Journal of Atmospheric and Oceanic Technology*, vol. 12, no. 2, pp. 317–329, 1995.
  - <sup>5</sup> G. Bazile Kinda and J. Bonnel, “Passive acoustic observations of tide height in the ivoire sea using ambient noise,” *The Journal of the Acoustical Society of America*, vol. 138, no. 3, pp. EL299–EL304, 2015.
  - <sup>6</sup> P. Felisberto, J.P. Silva, A.J. Silva, S.M. Jesus, I. Olivé, R. Santos, H. Quental-Ferreira, P. Pousão-Ferreira and M.E. Cunha, “Acoustic detection of bubbles in a pond covered by the seagrass *Cymodocea nodosa*,” accepted in *OCEANS, 2017 IEEE - Aberdeen*, , 2017.
  - <sup>7</sup> P. Felisberto, S. Jesus, F. Zabel, R. Santos, J. Silva, S. Gobert, S. Beer, M. Bjork, S. Mazzuca, G. Procacini, J. W. Runcie, W. Champenois, and A. V. Borges, “Acoustic monitoring of O<sub>2</sub> production of a seagrass meadow,” *Journal of Experimental Marine Biology and Ecology*, vol. 464, pp. 75 – 87, 2015.
-